LAPP-EXP 2001-01
Janvier 2001

The ATLAS detector

P. PERRODO

LAPP, IN2P3-CNRS, Chemin de Bellevue, BP110,
F-74941, Annecy-le-Vieux

abstract

The ATLAS detector, one of the two multi-purpose detectors at the Large Hadron Collider at CERN, is currently being built in order to meet the first proton-proton collisions in time. A description of the detector components will be given, corresponding to the most up to date design and status of construction, completed with test beam results and performances of the first serial modules.

Talk given at the Hadron Structure International Conference,
Stara Lesna, High Tatras Mountains,Slovakia, 2.-7. October 2000

The ATLAS detector

Pascal Perrodo[1]
LAPP, Laboratoire d'Annecy-le-vieux de Physique des Particules,
Chemin de Bellevue, 74941 Annecy, France

The ATLAS detector, one of the two multi-purpose detectors at the Large Hadron Collider at CERN, is currently being built in order to meet the first proton-proton collisions in time. A description of the detector components will be given, corresponding to the most up to date design and status of construction, completed with test beam results and performances of the first serial modules.

1 Introduction

The ATLAS detector is one of the multi-purpose detectors which will be installed at the LHC accelerator at CERN to study new physics phenomena produced in proton-proton collisions at $\sqrt{s} = 14$ TeV with expected luminosities of firstly 10^{33} cm^{-2}s^{-1} then 10^{34} cm^{-2}s^{-1}. The LHC is a factory for standard physics processes with orders of magnitudes above what has been or will be done before: at $\mathcal{L} = 10^{33}$ cm^{-2}s^{-1} the expected numbers of events per year for known processes are: 10^7 for Z $\rightarrow$ e$^+$e$^-$, 10^8 for W$^-$ $\rightarrow$ e$^-\bar{\nu}_e$, 10^{12} for b$\bar{b}$, 10^7 for t$\bar{t}$ and 10^9 for QCD jets with $p_T > 200$ GeV/c. The detector has been optimized for Higgs search over a wide mass range, but also for heavy Z and W-like objects, for supersymmetric particles search, compositeness, top quark study and CP violation in B decays. Theses topics require a good capability of reconstructing and measuring jets, E_T, E_T^{miss}, identify electrons and muons, b and $\tau^\pm$ jets. These studies led to the technical proposal for the detector [1] in 1994. About two or three years later appeared the Technical Design Reports (TDR) for each sub-detectors or sub-systems, describing the final design of the detector components in association with full size test beam prototype realisations. Nevertheless further optimizations or changes took place after the TDR issues and the first test beams. Most of them have been described in a special TDR dedicated to detector and physics performances [2].

Today the building of the ATLAS detector has started in order to meet the first LHC collisions in time. A description of the sub-detectors will be given below, in association with some results of the full size prototypes or the first serial components in test-beam and also some expected global performances. A general view of the detector showing all the sub-detectors without the muon system can be found in Figure 1 and a schematic of the muon system can be found in Figure 8. The description of the trigger and the data acquisition system will not be approached here but can be found in [3, 4].

---

[1] *E-mail address: pascal.perrodo@lapp.in2p3.fr*

2   The inner tracking detectors

The ATLAS inner tracking system [5, 6] is contained into a cylinder of 1.15 m radius and 7 m length. A superconducting solenoid provides a 2 T axial magnetic field (from a 8 kA current) for transverse momentum measurement. The location of this solenoid in front of the electromagnetic calorimeter has required a severe minimisation of the material to keep the calorimetric energy resolution performances. Therefore the solenoid is located in the cryostat vessel of the electromagnetic liquid argon calorimeter [7] making the economy of two vacuum walls.

The purposes of the inner tracking system consist in: (*i*) providing a recognition of the charged tracked produced in the collisions in the presence of numerous low transverse momentum tracks from minimum bias events at high luminosity (10^{34} cm^{-2}s^{-1}) and determine the tracks relevant for physics; (*ii*) measuring the helix parameters of the relevant tracks, i.e. their momentum and their impact parameter with precision in order to reconstruct secondary vertices; (*iii*) identifying electron against pion tracks. These requirements have to be fulfilled with the following constraints: (*i*) high occupancy of the trackers at high luminosity; (*ii*) high radiation levels due to low energy neutron and photon fluxes; (*iii*) keep as low as possible the amount of material in the tracker in order not to degrade the tracking or the calorimetric performances.

The system elaborated by the ATLAS collaboration consists of pixel detectors close to the interaction point, a semiconducting tracker at larger radius and a transition radiation detector(see Figure 2). In order to provide a uniform η (rapidity) coverage each of these three systems described below are composed of a barrel part at small rapidity and endcap-like parts at higher $|\eta|$.

2.1   The pixel detector

Included in a cylinder of 13 cm radius, the pixel system [8] is composed of three layers for the barrel part located at radii of 5,10 and 13 cm and five disks on each sides, insuring a coverage up to $|\eta| = 2.5$. It consists in an ensemble of about 1500 modules for the barrel part and 700 for the disks. Each module (identical for barrel and end-cap) is 6.24 cm long and 2.14 cm large, showing 61,440 pixels. One pixel is designed to size 50 μm in the $R - \phi$ direction and 400 μm in the z direction. The corresponding resolutions measured are typically 12 μm in the $R - \phi$ direction and 300 μm in z direction. In total the system contains 140 millions pixels.

The role of this sub-detector is to insured a very high granularity for precision measurements at the closest distance of the interaction point. The high granularity helps to keep the occupancy rate at an acceptable level (1% at high luminosity) and the three layers 3-dimensional coordinates determines the precision impact parameter, helping for B hadrons and $\tau^{\pm}$ tagging.

The p-spray insulation technique for irradiation protection has been demonstrated to work for 10 years of radiation (300 kGy and 5×10^{34} cm^{-1} neutron flux). Each module is readout by 16 chips which have been now moved to rad-hard technologies and the technique of bump-bonded (to achieve the required density of connections) has been demonstrated to work well.

2.2 The semiconducting tracker

Surrounding the pixel system the semiconducting tracker [6] consists in a barrel part made of four layers from radius 30 cm to 52 cm and in nine wheels on each side up to $z = 3.5$ m, providing an acceptance up to $|\eta| = 2.5$. Each individual module sizes about 6×6 cm^2 with 768 strips of 80 μm pitch on each side. The two sides glued back to back are rotated with an angle of 40 mrad insuring a stereo view. This allow to achieve a resolution of 16 μm in the $R - \phi$ direction and 600 μm in z direction. The end-cap part is based on the same principle and is made of wheels with inner radii and $|z|$ chosen to optimize the $|\eta|$ coverage.

The role of this silicon tracker is to provide eight coordinates per track, allowing to measure the momentum, the impact parameter in combination with the pixel system and give a good pattern recognition. In Figure 3 are given some results of simulations concerning the B-tagging performances: the distribution of the track significance (the signed track impact parameter divided by its estimated error) clearly shows the evidence of b jets for large values. The rejection power for light quark jets and gluon jets are also given as a function of the b tagging efficiency. This performance is crucial especially for the observation of a Higgs decay into $b\bar{b}$ in associated production [2].

2.3 The transition radiation tracker

The role of this detector [6] is to provide pattern recognition, track measurements and $e^{\pm}/\pi^{\pm}$ separation. As it is located at a larger distance from the interaction point, in order not to cope with an too high number of channels and high radiation levels, its technique is based on the use of small diameter (4 mm) straws filled with gas (Xe,CO$_2$,CF$_4$) and containing a small (30μm diameter) wire. The barrel part is made of about 50000 straws of 144 cm length and parallel to the LHC beam line, providing typically 36 hits measurements from $R = 56$ cm to 107 cm. Each z side consists in 18 wheels with a total of 420,000 radial straws (see Figure 2). The density of straws in the wheels as well as the wheel inner diameters have been chosen such a way that the number of crossed straws is constant over the full acceptance. The space between the straws is filled with a radiator. For the barrel it consists in a polypropylene fiber foam and of foils orthogonal to the beam line for the end-cap wheels. The radiation transition photons can be detected thanks to the presence of Xe gas. The photon energy distributions from test-beams for $e^{\pm}$ and $\pi^{\pm}$ can be seen in Figure 4 showing a good agreement with the simulation. This effect allows to provide a discrimination between electrons and hadrons shown in the same Figure.

The hit rate in the straws at design luminosity vary between 6 and 19 MHz. Hits above a given transition radiation threshold have a 1MHz rate. For TRT hits with a 12 MHz rate, a precision of 170μm on the position has been achieved. Combining all tracking subdetectors provides on the usual helix parameters [2] the following results at $\eta = 0$: $\sigma(p_T)/p_T^2 = 0.36$ TeV^{-1}, $\sigma(d_0) = 11\mu$m and $\sigma(z_0) = 87\mu$m.

3 The calorimeters

The choice made by ATLAS for the calorimetry (see Figure 5) consists in a lead-ℓAr (liquid argon) technique for the electromagnetic calorimeter and in a iron-scintillator for the hadronic one in the barrel part. In the more forward region where the radiation level is higher a calorimeter based on copper-ℓAr has been preferred. Finally at very large $|\eta|$ a ℓAr forward calorimeter based on rod-shaped electrodes take place. The performances of the designed detectors have been studied in [9] and [2].

3.1 The electromagnetic calorimeter

This detector, crucial for $e^{\pm}$ and photon identification consists in a ℓAr lead calorimeter with accordion shape absorber plates [10]. This feature gives a fast response time for the signal and insure a complete 2π coverage in ϕ (azimuthal angle). The lead thickness has been optimized as a function of η in terms of acceptable energy resolution (see Figure 5). The ℓAr gap sizes 2.1 mm in the barrel part and is variable in the end-cap region due to the special geometry. The electrode maintained between two absorbers by honeycomb spacers is made of three copper layers isolated by two kapton foils. The two external parts holds the high voltage (to insure a 10 kV/mm electrical field) and the median part reads the signal by capacitive coupling. The calorimeter is segmented into three longitudinal layers and the electrodes are segmented in η with a projective geometry. The first layer ($6X_0$) has a very fine segmentation in η ($\Delta\eta \approx 0.003$) allowing π^0 identification and precise position measurements. The middle layer (going up to $24X_0$) gives the core energy measurement of the shower and the back layer acts either as a pion veto for low energy electron showers or as a tail-catcher for high energy electrons.

The calorimeter is divided into a barrel part ($|\eta| < 1.475$) and the end-caps ($1.375 < |\eta| < 3.2$). Around $|\eta| = 1.4$ is located the crack between the barrel and the end-cap containing a scintillator to recover partially the energy deposited into it (see Figure 5). In the region $|\eta| < 2.5$ a presampler detector made of a pure ℓAr gap without absorber medium is located just behind the cryostat wall and in front of the calorimeter. Its role is to sample the shower just after it has started to develop in the inner detector and the cryostat walls. The signals are readout and amplified by bipolar shapers, sampled every 25 ns and stored into analog pipelines, waiting for level 1 trigger decision for digitization, making about 200,000 channels in total.

Full size prototype modules have been realized for the barrel (see Figure 6) and the end-cap. Associated test-beam results showed good agreement with expectations for position, energy resolution and energy linearity responses [11] The construction of the final modules has now started.

3.2 The hadronic end-cap calorimetry

Located just behind the end-cap electromagnetic ℓAr calorimeter each end-cap hadronic detector (see Figure 1) consists in two wheels of about 2 m diameter [10]. They cover a rapidity domain of $1.5 < |\eta| < 3.1$. The absorber is made with copper plates of 25 mm and 50 mm thickness. The gap between two absorbers is 8.5 mm wide filled

with 3 electrodes making a 1.8 mm individual gap. The two extreme electrodes are only used for holding the high voltage and the central one, based on the same principle as the electromagnetic electrode with three conducting layer reads the signal. Each wheel is divided into 32 mechanical modules in ϕ. Due to larger detector capacitance than the accordion part the signal is amplified by a cold electronics for noise reduction. Prototype have been built to validate the technique and building of serie modules have started. Test-beam results for these modules show results compatible with the designed expectations [12].

3.3 The forward calorimetry

Between $3.2 < |\eta| < 4.9$ is located a special calorimeter which has to face a very high level of radiation. In order to reduce the albedo from this calorimeter on the end-cap electromagnetic accordion part the forward calorimeter is placed at a larger distance from the interaction point than the former (see Figure 1). This detector [10] consists in three sections, the first one made in copper, the others in tungsten. In these matrices there are longitudinal tubes filled with rods put to high voltage. The gap between the tube and the rod is filled with ℓAr (250μm in the first section) making the sensitive ionizing medium. The chosen segmentation make in total about 3,500 channels. The construction of the modules is well advanced and test-beam results have shown nice performance results [13].

3.4 The tile calorimeter

The hadronic calorimetry for the barrel part will be achieved in ATLAS by a iron-scintillator based (called tiles) calorimeter [14]. The basic structure consists in 3 mm scintillating tiles and 14 mm iron plates making a periodic structure in z. Each tile is readout by two wavelength shifting fibers and two phototubes. In order to well cover the calorimetry the tile calorimeter consists in a barrel part and two extended part around the end-cap cryostats (see Figure 1). They are segmented into three layers sizing 1.4, 4.0 and 1.8 interaction lengths. The chosen granularity (0.1×0.1 in (η, ϕ)) represents about 10,000 channels. The barrel and the extended part are divided for mechanical reasons into 64 modules (see Figure 7). The phototubes and the front-end electronics are located in the girder making also the mechanical support of the structure. Building for the serie modules has started and recent test-beam results concerning calorimetry can be found in [15] as well as studies of the hadronic shower profiles [16] showing good agreement with simulations.

4 The muon spectrometer

Detection and measurement of muons is as important as electron ones. It will be achieved in ATLAS by a air toroidal magnetic field instrumented with precision tracking chambers and trigger chamber to make the muon spectrometer working as a stand alone detector [17]. The apparatus is divided into three parts, a barrel one covering the

domain $|\eta| < 1.0$ with a magnet system made of eight superconducting coils providing a peak value of about 4T field [18, 19]. In the interval $1.4 < |\eta| < 2.7$ the magnetic field is provided by two sets of end-cap coils [20] and the region in between it is made by a combination of both barrel and end-cap magnets. In the barrel the precision tracking is performed by three layers of monitored drift tubes (MDT) (see Figure 8) in two orthogonal directions. The chambers are placed parallel to the beam line. In the end-cap region the same chambers are used but placed orthogonal to the beam line. At higher rapidity values cathode strip chambers (CSC) with fine granularity are used to cope with high rates and background conditions. In total there are more than 10^6 channels in the muon system. The precision on the hit position reached with the MDT is 80μm. This can be achieved with an efficient alignment system using laser beams. In addition the muon system provides a level one trigger signal thanks to resistive plate chambers (RPC) in the barrel and thin gap chamber (TGC) in the forward region.

5   Conclusion

The progress of the ATLAS project is monitored using a detailed ATLAS-internal milestones procedure. At moment there are very good progress to be reported as all components of the detector are now in the construction phase. This gives good hope to see the detector ready to meet the first LHC collisions in time.

Acknowledgments

References

[1] ATLAS Collaboration, *ATLAS technical proposal*, CERN/LHCC/94-43

[2] ATLAS Collaboration, *Detector and physics performances technical design report*, 2 volumes, CERN/LHCC/99-14 and CERN/LHCC/99-15

[3] ATLAS Collaboration, *First-level trigger technical design report*, CERN/LHCC/98-14

[4] ATLAS Collaboration, *DAQ, EF, LVL2 and DCS technical design report*, CERN/LHCC/98-16

[5] ATLAS Collaboration, *Inner detector technical design report, vol1*, CERN/LHCC/97-16

[6] ATLAS Collaboration, *Inner detector technical design report, vol2*, CERN/LHCC/97-17

[7] *ATLAS central solenoid technical design report*, CERN/LHCC/97-21

[8] ATLAS Collaboration, *Pixel detector technical design report*, CERN/LHCC/98-13

[9] ATLAS Collaboration, *Calorimeter performance technical design report*, CERN/LHCC/96-40

[10] ATLAS Collaboration, *Liquid argon calorimeter technical design report*, CERN/LHCC/96-41

[11] R. Zitoun, *Preliminary results on the ATLAS liquid argon electromagnetic calorimeter*, ICHEP2000, Osaka, talk 12c-05
C. Clément, *Performance of the ATLAS electromagnetic calorimeter: tests of barrel and end cap modules*, CALOR2000, Annecy, 9-14 october 2000.

[12] A. Minaenko, *Test-Beam results for first serial module of the ATLAS hadronic end-cap calorimeter*, CALOR2000, Annecy, 9-14 october 2000

[13] D. Bailey, *Test beam measurements of the response of the ATLAS forward calorimeter*, CALOR2000, Annecy, 9-14 october 2000

[14] ATLAS Collaboration, *Tiles calorimeter technical design report*, CERN/LHCC/96-42

[15] M. David, *Instrumentation and performance of the first TILECAL*, CALOR2000, Annecy, 9-14 october 2000

[16] ATLAS Tile collaboration, *Hadronic shower development in iron-scintillator tile calorimeter*, CERN-99-055

[17] ATLAS Collaboration, *Muon spectrometer technical design report*, CERN/LHCC/97-22

[18] ATLAS Collaboration, *Magnet system technical design report*, CERN/LHCC/97-18

[19] ATLAS Collaboration, *Barrel toroid technical design report*, CERN/LHCC/97-19

[20] ATLAS Collaboration, *End-cap toroid technical design report*, CERN/LHCC/97-20

Hadronic Tile
Calorimeters

EM Accordion
Calorimeters

Forward LAr
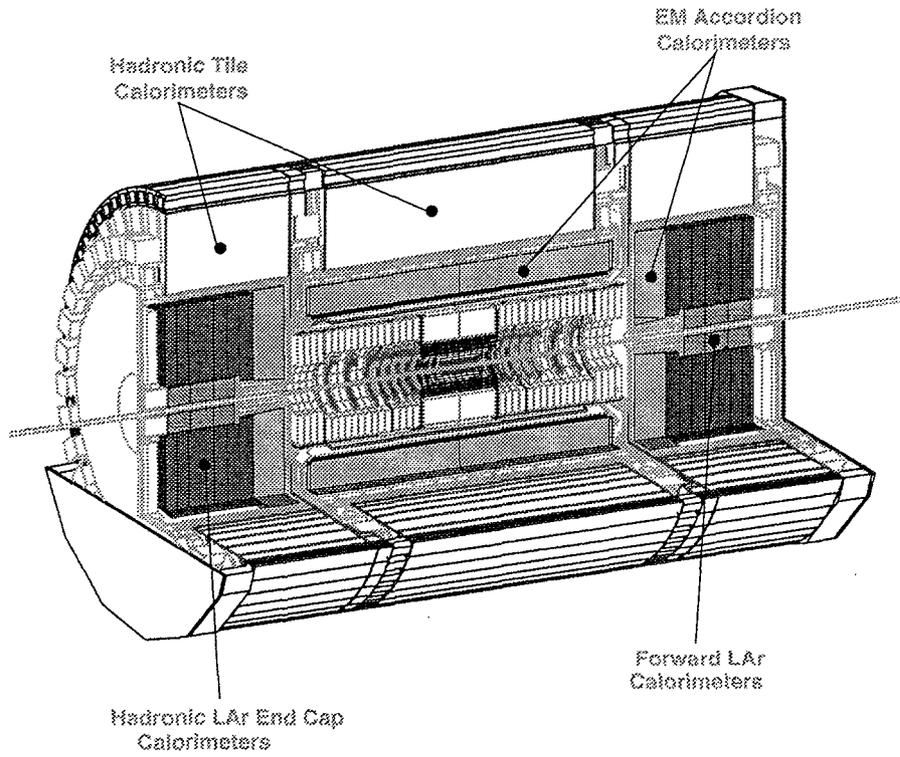Calorimeters

Hadronic LAr End Cap
Calorimeters

Fig. 1: General view of the ATLAS detector without the muon spectrometer, showing the central tracking detector and the calorimeters.
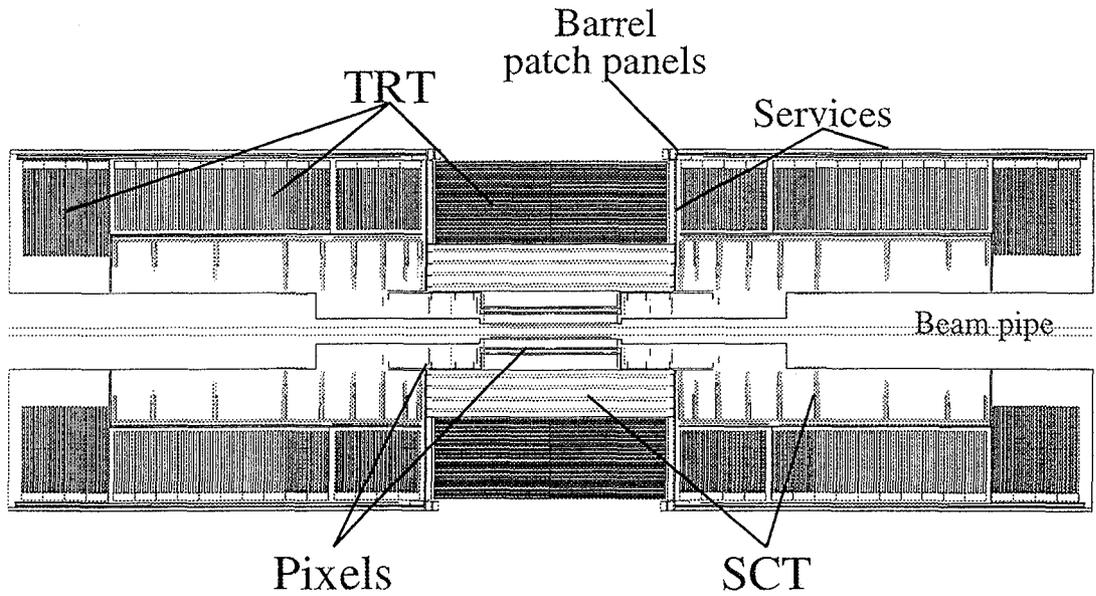
Fig. 2: General view of the ATLAS inner tracker. The charged tracks meet successively the pixel detector, the silicon detector (SCT) and the transition radiation detector (TRT). The latest is in charge of identifying $e^{\pm}$.
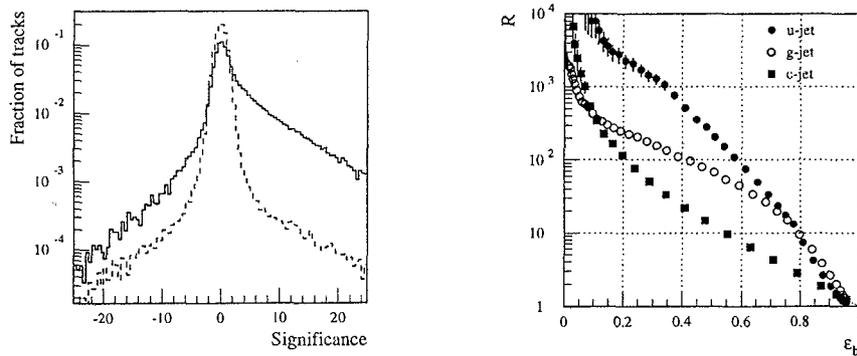

Fig. 3: Left: Signed impact parameter for the tracks divided by its error (called significance). The solid curve is for b jets, the dashed one for u jets. (The two curves are normalised to the same area. Right: Rejection factor R for various backgrounds (u,c,gluon jets) as a function of the b jet tagging efficiency ε_b.
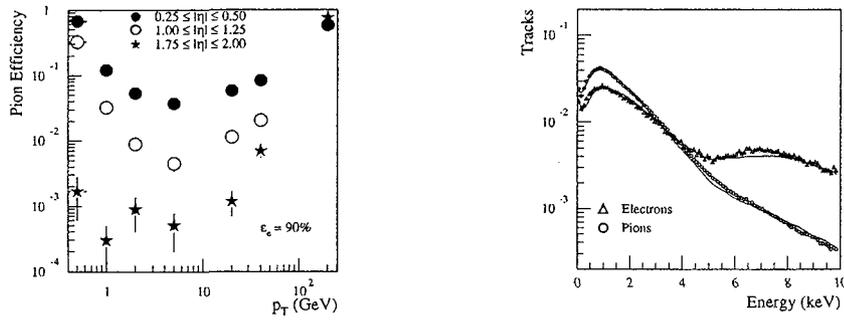
Fig. 4: Left: Tagging efficiency for $\pi^{\pm}$ as a function of its transverse momentum p_T, assuming a tagging efficiency for $e^{\pm}$ of 90%. (Plotted here for various $|\eta|$ intervals.) Right: Energy deposited in the straws for $e^{\pm}$ and $\pi^{\pm}$. The dots and triangles are test-beam data, the solid lines are simulations.
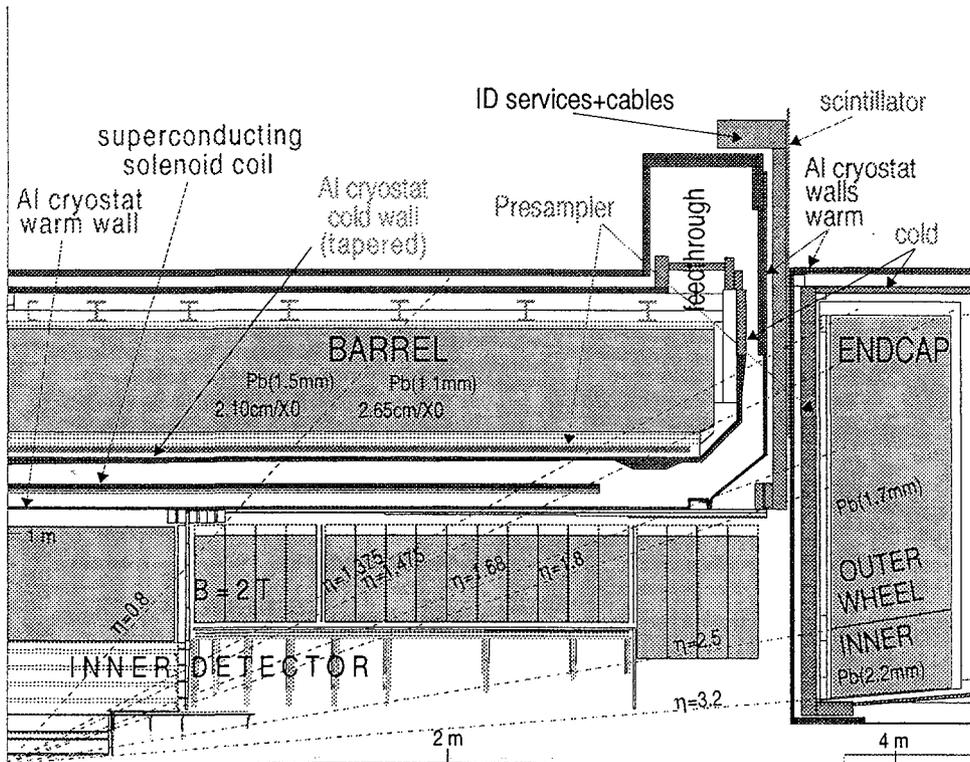

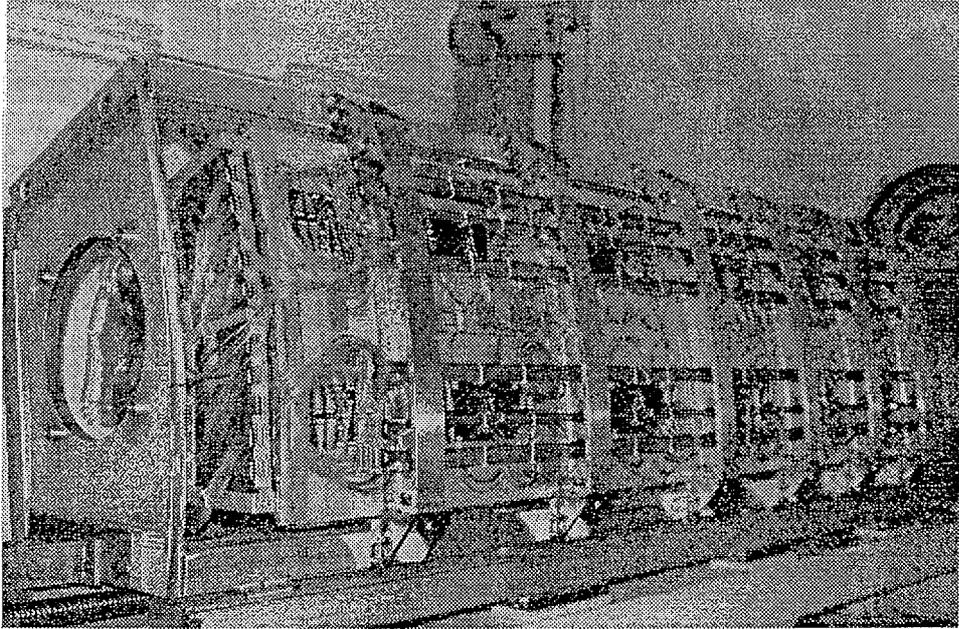Fig. 5: General $R - z$ view of the ATLAS electromagnetic calorimetric system.

Fig. 6: View of the full size prototype module ($2\pi/16$ in ϕ) of the electromagnetic liquid argon barrel calorimeter. The outer rings supporting the detector can be seen on the larger radius face as well as the readout cables.
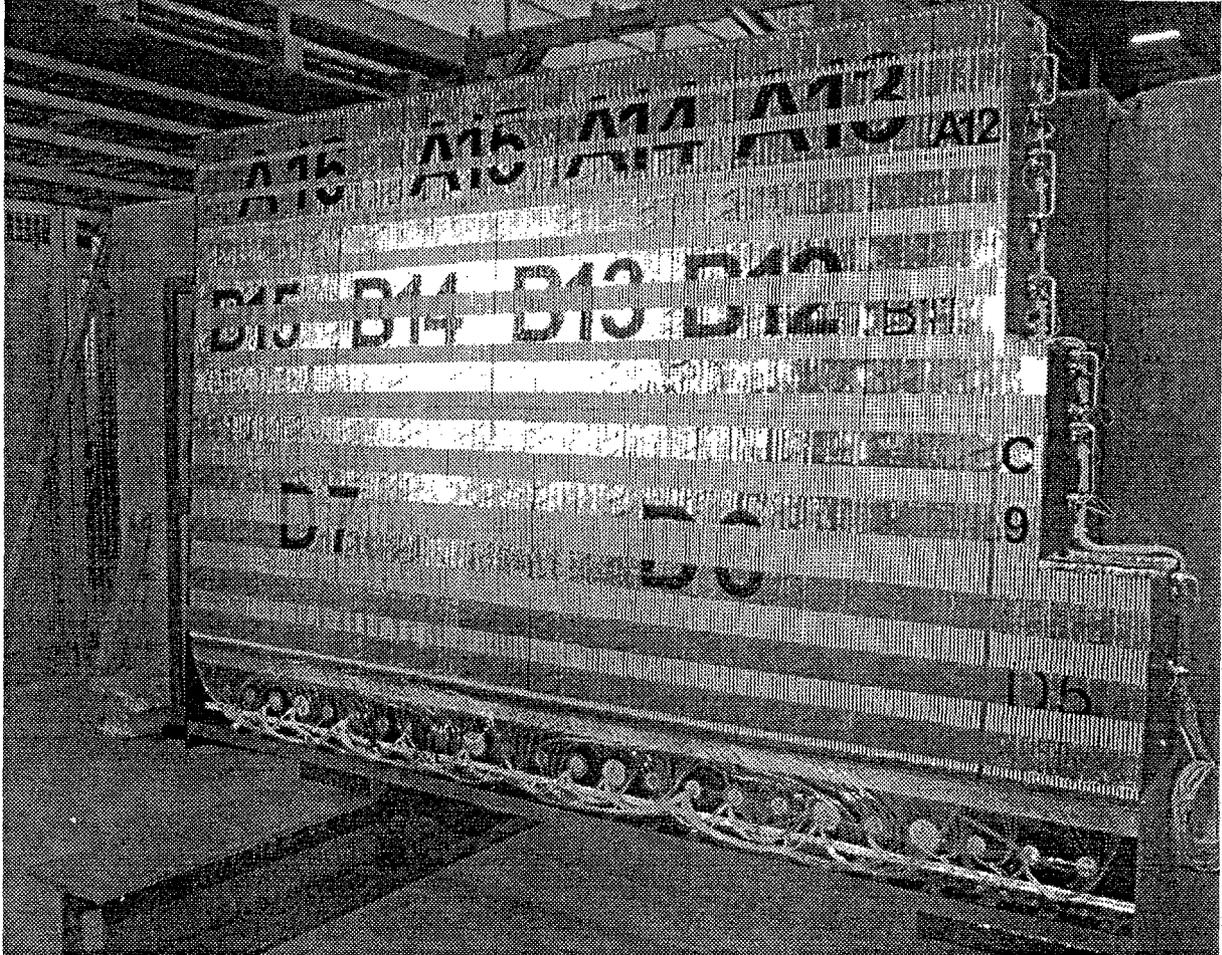
Fig. 7: View of a module ($2\pi/64$ in ϕ) of the extended tile calorimeter. The larger radius part of the module consists in a girder which supports the mechanics and includes the fibers collecting the light, the photomultiplier tubes and the front-end electronics.
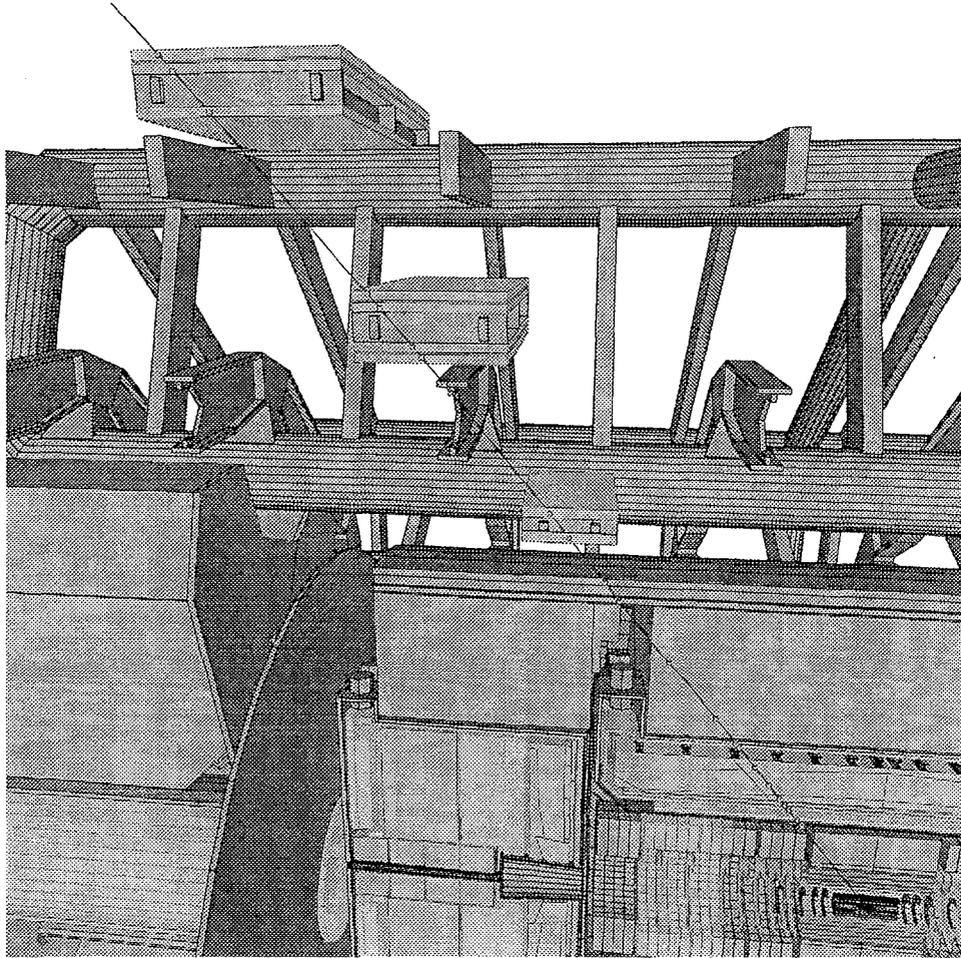
Fig. 8: General $3 - d$ view of the muon toroid ATLAS subdetector. A muon track from the interaction point travelling accross the detector meets successively three layers made of monitored drift tubes chambers (MDT) and resistive plate chambers (RPC) used for triggering.